Metallic lead nanospheres discovered in ancient zircons

Monika A. Kusiak[a,b,1], Daniel J. Dunkley[c], Richard Wirth[d], Martin J. Whitehouse[b], Simon A. Wilde[c], and Katharina Marquardt[d,e]

[a]Institute of Geological Sciences, Polish Academy of Science (ING PAN), 00-818 Warsaw, Poland; [b]Department of Geosciences, Swedish Museum of Natural History, SE104 05 Stockholm, Sweden; [c]Department of Applied Geology, Curtin University, Perth, WA 6845, Australia; [d]Experimental Geochemistry, GeoForschungsZentrum Potsdam, 3.3 D-14473 Potsdam, Germany; and [e]Bayerisches Geoinstitut, Universität Bayreuth, D-95440 Bayreuth, Germany

Edited by Richard W. Carlson, Carnegie Institution of Washington, Washington, DC, and approved March 11, 2015 (received for review August 8, 2014)

Zircon ($ZrSiO_4$) is the most commonly used geochronometer, preserving age and geochemical information through a wide range of geological processes. However, zircon U–Pb geochronology can be affected by redistribution of radiogenic Pb, which is incompatible in the crystal structure. This phenomenon is particularly common in zircon that has experienced ultra-high temperature metamorphism, where ion imaging has revealed submicrometer domains that are sufficiently heterogeneously distributed to severely perturb ages, in some cases yielding apparent Hadean (>4 Ga) ages from younger zircons. Documenting the composition and mineralogy of these Pb-enriched domains is essential for understanding the processes of Pb redistribution in zircon and its effects on geochronology. Using high-resolution scanning transmission electron microscopy, we show that Pb-rich domains previously identified in zircons from East Antarctic granulites are 5–30 nm nanospheres of metallic Pb. They are randomly distributed with respect to zircon crystallinity, and their association with a Ti- and Al-rich silica melt suggests that they represent melt inclusions generated during ultra-high temperature metamorphism. Metallic Pb is exceedingly rare in nature and previously has not been reported in association with high-grade metamorphism. Formation of these metallic nanospheres within annealed zircon effectively halts the loss of radiogenic Pb from zircon. Both the redistribution and phase separation of radiogenic Pb in this manner can compromise the precision and accuracy of U–Pb ages obtained by high spatial resolution methods.

metallic Pb | nanospheres | zircon | Antarctica | early Earth

Zircon is the mineral of choice for precisely determining the timing of both magmatism and metamorphism in a wide range of geological samples as well as providing constraints on the source and time of deposition of clastic sedimentary rocks. Accurate zircon geochronometry is facilitated by zircon having a lattice structure that is stable over a wide range of temperatures and pressures (1), together with the fact that whatever Pb is present derives almost entirely from radioactive decay of U and Th. During its growth, zircon incorporates small amounts of nonformula elements, including Hf, Ti, and Y, and rare earth elements, U and Th, but generally excludes Pb. This incompatibility of Pb raises questions about how radiogenic Pb is retained in zircon, especially through geological events where elevated temperature, fluid activity, and deformation can enhance element mobility. Furthermore it has been established that an irregular redistribution of lead in metamorphic zircon can degrade the precision and accuracy of U–Pb isotopic data, in extreme cases leading to spurious ages (2, 3).

Experimental and natural studies have revealed that element mobility in zircon is strongly dependent on the accumulation of α-recoil damage (4, 5). Multiple α-decay events along the U and Th decay chains leading to stable daughter Pb isotopes destroy the crystal lattice, creating amorphous domains tens of nanometers in size (6, 7). As the number of these domains increases over time, they begin to overlap until the so-called first percolation point is reached at 2.2×10^{18} α-decay events per gram (8). At this point, the zircon is considered "metamict," and the diffusivity of Pb and other elements is enhanced compared with diffusion in crystalline zircon. Therefore, loss of Pb from metamict zircon is highly likely and is further enhanced by the chemical instability of amorphous materials (9). Although healing of radiation damage occurs during metamorphism, its degree and nature is dependent on the U content, the density of radiation damage, and the temperatures involved. Zircon with concentrations of U and Th typical of those found in common rocks (less than 0.5%) will not accumulate significant radiation damage above ca. 350–400 °C (5, 10). However, in zircon that is already metamict, complete recovery through thermal annealing will not occur at these temperatures (5). During high-temperature metamorphism (>600 °C), there is a complex interplay of factors at work on zircon that can act both for and against preservation of initial U–Th–Pb isotopic signatures and thus its ability to preserve accurate age information.

Migration of radiogenic Pb in zircon has been established by several studies that reveal heterogeneous distribution of Pb on various length scales. These include transmission electron microscopy (TEM) studies (11), ion microprobe imaging (2) and tomography (12), and atom probe tomography (13), the latter study suggesting that migration occurs by diffusion of Pb through crystalline zircon into noncrystalline domains produced by α-recoil damage.

In the Napier Complex of Enderby Land, East Antarctica, metasedimentary and metaigneous gneisses preserve zircon ages greater than 3.8 Ga (14, 15). The central–western part of the

Significance

Metallic lead nanospheres have been discovered in ancient (>3.4 Ga) zircon grains from an Archean (2.5 Ga) high-grade metamorphic terrain in East Antarctica. Native Pb is present as 5–30 nm nanospheres, commonly in association with an amorphous silica-rich phase, along with titanium and aluminium-bearing phases. Together, these phases form nanoinclusions generated during the recovery of crystallinity in radiation-damaged zircon under high-grade metamorphic conditions. Once formed, the entrapment of nanospheres in annealed zircon effectively arrests Pb loss, explaining why zircon that has experienced such extreme conditions is not completely reset to its metamorphic age. The heterogeneous distribution of Pb can, however, affect isotopic measurement by microbeam techniques, leading to spurious age estimates. Metallic Pb is extremely rare in nature and has never previously been observed in high temperature rocks.

Author contributions: M.A.K., D.J.D., and R.W. designed research; M.A.K., D.J.D., R.W., M.J.W., S.A.W., and K.M. performed research; M.A.K., R.W., and K.M. analyzed data; and M.A.K., D.J.D., R.W., M.J.W., S.A.W., and K.M. wrote the paper.

The authors declare no conflict of interest.

This article is a PNAS Direct Submission.

[1]To whom correspondence should be addressed. Email: monika.kusiak@twarda.pan.pl.

Napier Complex experienced an early metamorphic event at ~2.8 Ga (16) and then underwent ultra-high temperature (UHT) metamorphism at ca. 2,550–2,480 Ma (17), with peak temperatures of ~1,050–1,120 °C and pressures of 7–11 kbar (16). The isotopic complexity of zircon grains from Enderby Land was recognized in the earliest studies that used secondary ion mass spectrometry (SIMS) for U–Pb dating (18, 19). The reliability of the oldest zircon ages, which include some reversely discordant analyses (i.e., with U–Pb ages older than $^{207}Pb/^{206}Pb$ ages), has been questioned based on evidence from ion imaging for disturbance of the U–Pb system (2). This is important because $^{207}Pb/^{206}Pb$ ages are generally considered to be more robust than U–Pb ages for older zircons. However, if radiogenic Pb has been decoupled from its parent U and not locally incorporated into the crystal lattice during an ancient geological event, when radiogenic $^{207}Pb/^{206}Pb$ values are significantly higher than at present, reverse discordance and spuriously old $^{207}Pb/^{206}Pb$ age estimates may result (2, 3, 18).

Results

TEM images reveal that zircons from the Napier Complex that have previously been shown by ion imaging to incorporate unsupported radiogenic Pb (2, 3) contain randomly distributed, 5–30-nm spherical lead inclusions. They occur either as individual droplets or in polyphase inclusions 20–80 nm across that also contain amorphous silica-rich and unidentified Ti–Al-rich phases (Fig. 1). Where inclusions contain multiple phases, Pb occurs as single or multiple nanospheres without crystal facets (Fig. 2 *A–D*). No hydrous Pb phase(s) or voids large enough to penetrate the focused ion beam (FIB) foils were found.

Considering the absence of sulfur, phosphorus, or other elements commonly associated with Pb minerals, the spectra indicate that the Pb-rich phase is either Pb–oxide, Pb–silicate, or native metal. To distinguish between these possibilities, diffraction patterns of the Pb nanospheres were calculated by Fast Fourier Transform (FFT) from high-resolution lattice fringe images. Thirty-five individual Pb nanospheres were examined. Diffraction patterns indicate that the Pb nanospheres are randomly oriented with respect to crystallographic axes, demonstrating that they are individual crystals, not atoms concentrated in the crystal lattice of host zircon. From a total of 31 individual lattice fringe measurements, five sets of d-spacings were identified (Table 1). The length of the different vectors defining the d-spacings were compared with the calculated d-spacings of pure lead (20), Pb–oxides (21–24), and trigonal (24) and hexagonal (25) Pb–silicate (Table 1). The number and length of measured d-spacings match the cubic structure of native Pb. Lead–oxide and Pb–silicate phases listed in Table 1 would exhibit additional, longer d-spacings, which were not observed. Three of the high-resolution images produced a set of three lattice fringes that could be completely indexed. There are two features required for cubic symmetry: (*i*) All vectors have lengths of 1.78 Å (in agreement with lead), and (*ii*) the angles between planes are 60°; an example is presented in Fig. 2*E*. Hexagonal symmetry [such as that possessed by the Pb–silicate $Pb_{21}(Si_7O_{22})_2Si_4O_{13}$] also has 60° angles but only in the [0001] zone axis pattern. The (30, 30) reflection (with a d-spacing of 2.86 Å) and its permutations show sixfold symmetry. However, in a simulated electron diffraction pattern with zone axis [0001] (i.e., the zone axis that would apply for that indexing), additional reflections, such as [–110–1] (and its permutations), with a d-spacing of 8.59 Å, are predicted. These reflections were not observed in the diffraction patterns from the Pb nanospheres. The diffraction pattern in Fig. 2*F*, in a different zone axis [100], can only be indexed as cubic Pb. As noted above, an additional strong argument for the Pb nanospheres being cubic is the fact that there were only five different sets of d-spacings, with the largest being 2.83 Å (Table 1), consistent with cubic symmetry. If there was an orientation

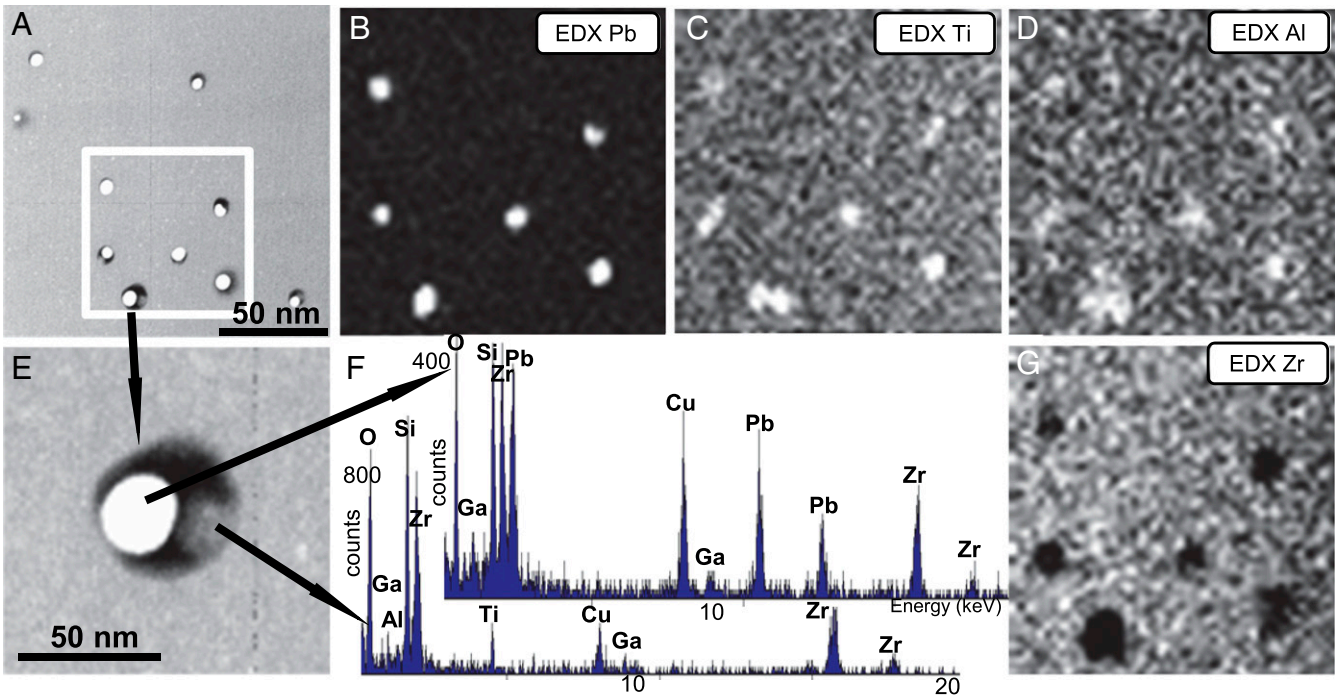

Fig. 1. (*A*) High-angle annular dark-field (HAADF) TEM image showing Pb nanospheres in Si-rich glass together with unidentified Ti–Al-rich phases. The white box represents the area covered by *B–D* and *G*. (*B–D* and *G*) Element maps for Pb, Ti, Al, and Zr, respectively. (*E*) Enlargement of one area with native Pb embedded in a melt inclusion. (*F*) EDX spectra of zircon rich in Pb (top spectrum) and the silicate matrix enriched in Ti–Al (bottom spectrum). Two spectra in Fig. 1*F* show that there is a difference in Zr intensity between zircon and the silicate melt in respect to Ti and Al. As the foil that constitutes the sample is ~150 nm thick and the average Pb nanosphere diameter is 20 nm, there will always be a substantial contribution of Zr–Si–O X-ray intensity coming from the matrix.

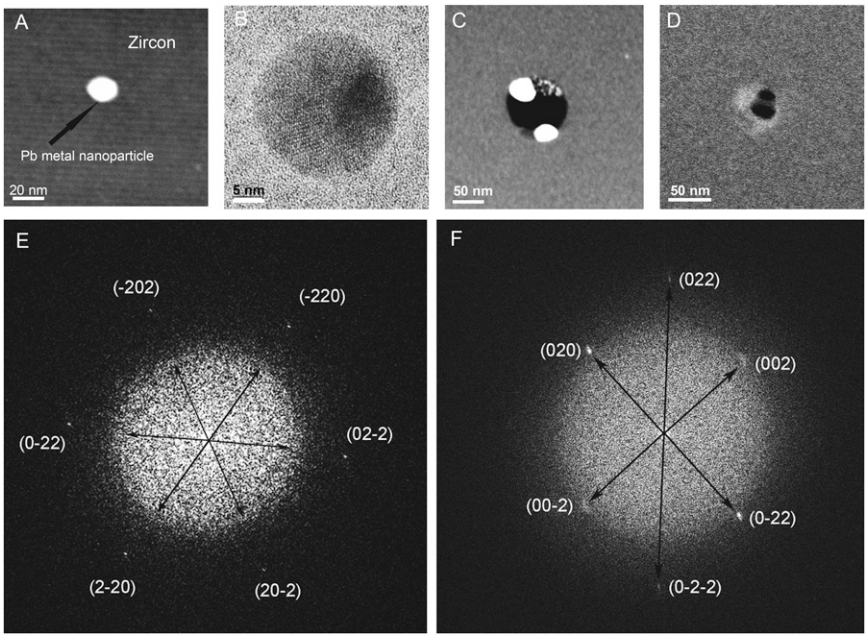

Fig. 2. (*A*) HAADF TEM image of Pb nanosphere in zircon. (*B*) HRTEM image of the Pb nanosphere shown in *A*. (*C–E*) HAADF TEM images of different examples of Pb nanospheres. (*C*) Two ca. 25 nm Pb metal particles together with many tiny Pb particles (<3 nm) enclosed in silica-rich glass (dark contrast). (*D*) Bright-field image of two Pb nanospheres in the stage of joining together but still separated by Si glass. (*E*) Diffraction pattern of the Pb nanosphere with the zone axis [–1–1–1] indexed as cubic Pb with angle of 60° and 1.78 Å d-spacing. (*F*) Diffraction pattern of the Pb nanosphere with the zone axis [100].

relationship between zircon and the Pb nanospheres, it should be possible to observe at least very weak diffraction spots in the diffraction images. These were never observed. Furthermore, if Pb–oxide or Pb–silicate were present, the d-spacings would be larger. From these observations, the only possible conclusion is that the nanospheres are composed of the native Pb.

The establishment that the Pb nanospheres belong to the cubic system eliminates the orthorhombic or tetragonal common oxides (PbO, PbO_2, or Pb_3O_4), as well as the monoclinic ($PbSiO_4$), orthorhombic ($PbSiO_3$, $Pb_{11}Si_3O_{17}$), trigonal ($Pb_3Si_2O_7$), and hexagonal [$Pb_{21}(Si_7O_{22})_2Si_4O_{13}$] Pb silicates. Hence, native lead is the only possible material that can constitute the nanospheres. When areas of zircon with variable degrees of crystallinity were examined, it was found that the nanospheres are concentrated in domains of lower crystallinity (Fig. 3*A*). Importantly, electron diffraction patterns of the host zircon confirm its crystalline state (Fig. 3 *B* and *C*), with varying degrees of radiation damage, as indicated by the smeared-out scattered reflections (Fig. 3 *D* and *E*) defining a mosaic crystal.

Discussion

The retention of radiogenic Pb in zircon is controlled by three main factors: the diffusivity of Pb in crystalline zircon, enhanced diffusivity in areas where domains of α-recoil damage overlap, and the recovery of radiation-damaged zircon through recrystallization or thermal annealing. Previously, Pb particles consisting of Pb–oxide and Pb–phosphate have been observed in synthetic zircon (26, 27). However, the reduced nature of native Pb documented here, along with the absence of nonradiogenic ^{204}Pb (2), argues against the action of external agents such as

Table 1. d-spacing of analyzed Pb nanospheres compared with published values for native Pb, Pb–oxides, and Pb–silicates

d_{hkl} observed, Å	Pb cubic	PbO_2 orthorhombic	PbO orthorhombic	Pb_3O_4 tetragonal	$Pb_3Si_2O_7$ trigonal	$Pb_{21}(Si_7O_{22})_2Si_4O_{13}$ hexagonal
*a_0 = 4.97 Å	a_0 = 4.9505 Å	a_0 = 4.9858 Å	a_0 = 5.8952 Å	a_0 = 8.8118 Å	a_0 = 10.1264 Å	a_0 = 9.9244 Å
		b_0 = 5.9590 Å	b_0 = 5.4930 Å	b_0 = 8.8118 Å	b_0 = 10.1264 Å	b_0 = 9.9244 Å
		c_0 = 5.4626 Å	c_0 = 4.7544 Å	c_0 = 6.5639 Å	c_0 = 38.6780 Å	c_0 = 34.2357 Å
		2.9795 (020)	2.9476 (200)	2.9034 (112)	2.9230 (300)	3.0371 (124)
2.83 *n* = 7 (SD = 0.03)	2.858 (111)					2.8649 (300)
		2.7310 (002)	2.7465 (020)	2.7863 (310)		
		2.4929 (200)	2.4896 (120)	2.5216 (212)		
2.44 *n* = 12 (SD = 0.07)	2.475 (020)	2.3952 (102)	2.3782 (021)	2.4437 (230)	2.4842 (223)	2.4746 (221)
				2.0883 (041)		
		2.1196 (211)		2.0768 (330)		
1.99 *n* = 5 (SD = 0.09)	2.021 (211)	2.0132 (022)	2.0460 (112)	2.0320 (411)	2.009 (321)	
1.75 *n* = 6 (SD = 0.01)	1.750 (022)	1.7591 (212)	1.7974 (022)	1.7907 (412)		
1.52 *n* = 1	1.565 (113)	1.5290 (132)	1.5146 (302)	1.5111 (350)	1.4407 (431)	

An asterisk indicates calculation from d-spacing. *n*, number of measurements; SD, standard deviation of measurements. From all measurements, only five different sets of d-spacings were obtained (first column), and these indicate cubic crystallographic symmetry. In all other crystal structures for Pb–oxide and Pb–silicate, d-spacings much larger than 2.83 Å should be observed. Nanospheres shown in Fig. 2 *E* and *F* can be only indexed as cubic Pb.

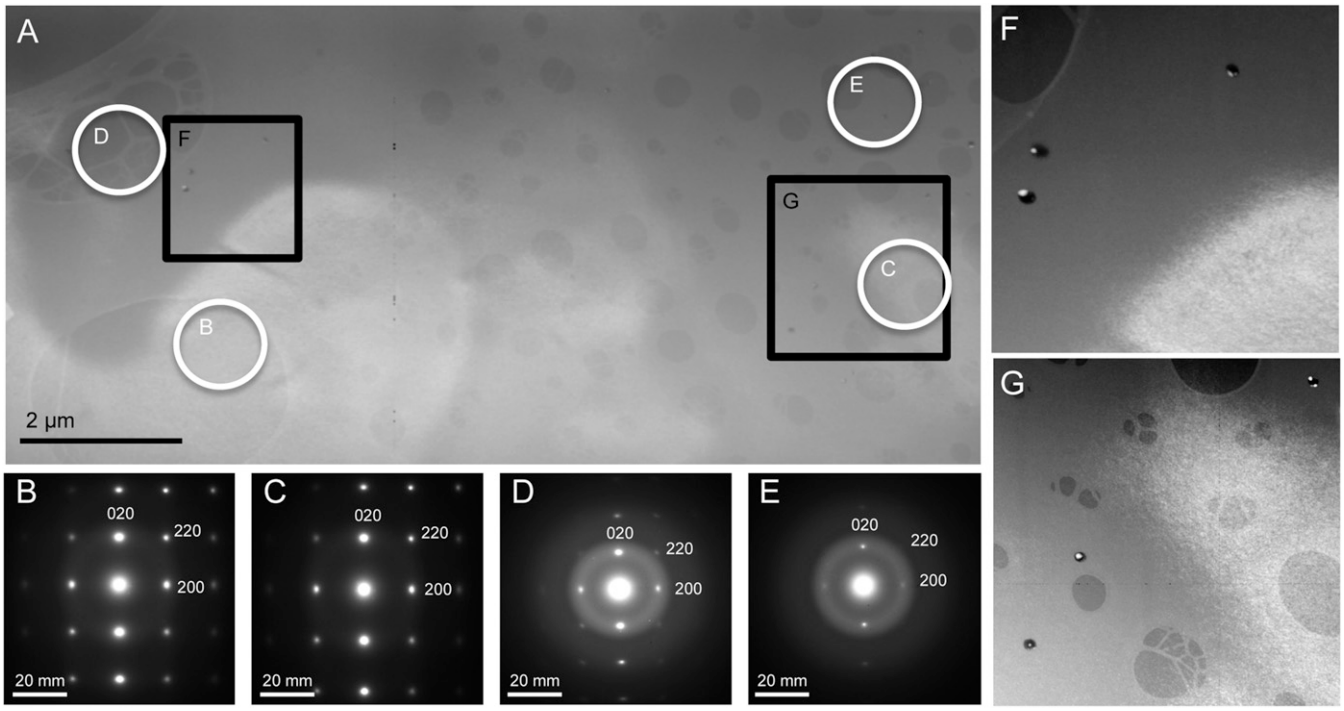

Fig. 3. (*A*) HAADF image displaying an overview of the TEM zircon foil. Differences in contrast represent areas of different irradiation damage in zircon. White circles *B*–*E* show areas where diffraction patterns were acquired. Black squares *F* and *G* show locations of the magnified HAADF images *F* and *G*, respectively. (*B*–*E*) Zircon electron diffraction patterns acquired with identical [001] zone axes. (*B* and *C*) More crystallized areas of zircon. (*D* and *E*) Intensive radiation damage from radiogenic decay visible as a strong decrease of X-ray scattering intensity and simultaneous increase of broad scattering intensity due to the increasing amount of noncrystalline material. (*F* and *G*) Images showing the presence of Pb only in the amorphous areas.

percolating fluids or melts in the formation of the nanospheres. Consequently, we suggest that thermal annealing is the sole agent of damage recovery and element mobilization in zircon with the Pb nanospheres. Because the mobility and compatibility of Pb is greatly enhanced in amorphous damaged zircon, the annealing process will concentrate Pb into these domains. It is likely that recovery will progress from the margins of predominantly crystalline domains, which can survive in parts of the zircon crystal with lower U and Th contents, into the more amorphous domains. In such cases, it is expected that crystal recovery along reaction fronts would force Pb into the unrecovered domains, leaving the healed domains Pb-free. This likely explains why the more crystalline domains are free of Pb nanospheres (Fig. 3). Importantly, whereas some of the differences in crystallinity observed in Fig. 3 may have been preserved through the annealing process, some, if not all, of the differences were likely produced by the accumulation of further radiation damage, owing to the geologically ancient timing of the metamorphism that induced annealing.

To account for the observations, we propose a thermal annealing model for crystal recovery and phase separation. Annealing involves the recovery of crystallinity in metamict zircon (Fig. 4*A*). At the first and second percolation thresholds, amorphous zircon makes up 30% and 70% of the zircon volume, respectively (28). According to calculation of the alpha-dose at the time of metamorphism (Table 2), two of the three zircons analyzed in this study were metamict. However, the zircon with the lowest ^{238}U content (165 ppm) may not have been, indicating that damage accumulation above the first percolation threshold is not a prerequisite for the formation of Pb nanospheres. Even in highly metamict zircon, nanoscale "islands" of crystallinity have been observed (29), and they would act as nucleation sites for lattice recovery. In such cases, recovery would occur until the crystalline domains merge and percolation is lost, trapping Pb in isolated amorphous domains. At a critical concentration, Pb, Si, and other elements that cannot be accommodated in the zircon structure formed inclusions of new mineral phases (Fig. 4*B*). It is unknown what solid or liquid phases may have been present at the high temperatures that were prevalent when the inclusions formed; however, the polyphase nature of the inclusions, the amorphous nature of the silica-rich phase, and the low melting point of metallic lead (327.5 °C at 1 atmosphere) suggest that coexisting silicate and lead melts were present at some stage. The presence of nanospheres of Pb indicates the separation of a metallic liquid phase from a silicate before the crystallization of native Pb. Once

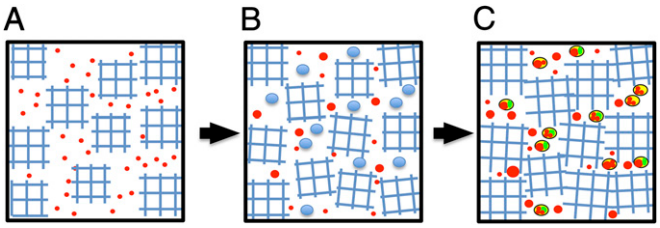

Fig. 4. Model of Pb nanosphere formation. (*A*) Zircon structure damaged by radioactive decay leaving "crystalline islands." Radiogenic Pb (red) is distributed in the noncrystalline areas. (*B*) During heating, individual incompatible elements, including lead, are concentrated in the noncrystalline areas forming melt inclusions (blue). Larger lead spheres form at the expense of smaller ones, thus minimizing surface energy (Ostwald ripening). (*C*) During cooling, the metal melt (Pb) separates from the Si-rich phase, forming nanospheres; Pb clusters are formed and are commonly associated with silica melt (yellow) locally enriched in Al and Ti (green). The spherical shape of the silicate–Pb inclusions suggests a melt at peak metamorphic conditions. Finally, the zircon crystalline islands grow and join together, forming a mosaic crystal.

Table 2. Radiation dosage calculation

Alpha-dose calculation	n3847-30	n3852-08	n3844-47
^{238}U, ugg^{-1}	165	4,917	1,614
^{232}Th, ugg^{-1}	81	211	378
Upper intercept ^{207}Pb/^{206}Pb age, Ma	3,300	2,810	3,680
Dose since upper intercept age	3.0×10^{18}	3.4×10^{19}	9.4×10^{19}
Dose since metamorphic age, 2,500 Ma	2.0×10^{18}	2.8×10^{19}	5.1×10^{19}
Dose radiation between formation and metamorphism	1.0×10^{18}	5.2×10^{18}	4.3×10^{19}
	Grain did not reach the first percolation point Not metamict	Grain could have reached the first percolation point, but not the second Metamict	Grain reached second percolation point Highly metamict grain

phase separation occurred, the Pb droplets embedded in silica melt inclusions grew in size and decreased in number through Ostwald ripening, thus minimizing surface energy. The presence of Al- and Ti-bearing phases may also be attributed to crystallization from a silicate melt (Fig. 4*C*). These and other elements that may have been originally compatible in the zircon structure when it first formed would have migrated along with incompatible Pb into nanoinclusions during annealing, possibly due to changes in compatibility, as the conditions of zircon annealing may not have been the same as those under which zircon initially grew (e.g., where lowering the temperature would reduce Ti solubility in zircon). Indeed, silicate melt inclusions in zircon, both glassy and crystalline, are well documented in the literature (30).

The native Pb nanoparticles observed in our study represent much higher concentrations of Pb than in the clusters observed in a recent atom probe study of a metamorphosed Hadean zircon (13) and are more heterogeneously distributed. In that study, a typical "Pb cluster," with a maximum concentration of about 0.2% Pb, contains about 4,000 atoms, and such clusters are distributed tens to hundreds of nanometers apart. Such small degrees of Pb heterogeneity would not affect SIMS analyses to any significant degree given the micrometer scale of the analytical spots. However, a sphere of crystalline lead 20 nm across (typical for the nanoinclusions observed in this study) composed of ^{206}Pb only (for ease of calculation) contains about 4.75×10^{-17} g or 139,000 atoms and is derived from a much larger volume of the host zircon. To understand how large a volume of zircon is required to produce such a nanosphere, we have calculated the values for examples of zircon with observed inhomogeneous Pb. For one example, the lowest concentration of ^{238}U in zircon as estimated by spot analysis (3), in which Pb inclusions were observed by SIMS mapping, is 165 μgg^{-1} (grain n3847-30). The volume of zircon associated with each ^{206}Pb sphere can be derived from the concentration of ^{238}U remaining in zircon at the present day, the age of formation of the Pb nanosphere (i.e., about 2.5 Ga), and the age at which the zircon first formed. Assuming this zircon had grown at the upper intercept age of 3.3 Ga (2), the concentration of radiogenic ^{206}Pb accumulated by 2.5 Ga would be 32 μgg^{-1}. Each 20-nm-wide nanosphere of ^{206}Pb would be derived from a spherical volume of zircon 792 nm in diameter, with a corresponding density of 3.8 Pb nanospheres per cubic micrometer of zircon. In this case, the maximum accumulated α-decay dose (which assumes that for the entire period between zircon formation at 3.3 Ga and metamorphism at 2.5 Ga, the zircon resided at temperatures low enough for damage to accumulate) is about 1.0×10^{18} events per gram, lower than the 2.2×10^{18} events per gram required for the zircon to become metamict (at the first percolation point). This demonstrates that the condition of complete metamictisation is not a prerequisite for the development of Pb melt inclusions (Table 2). In an example of zircon with higher U and observed Pb heterogeneity, (n3844-47), with 4,614 μgg^{-1} ^{238}U and an upper intercept age of 3.7 Ga, the concentration of radiogenic ^{206}Pb accumulated by 2.5 Ga would be 1,366 μgg^{-1}, with each ^{206}Pb sphere derived from a spherical volume of zircon 226 nm in diameter, corresponding to a density of 163 Pb spheres per cubic micrometer of zircon. In both cases, Pb inhomogeneity on the scale of a few tens of nanometer would be readily observable during analysis under a SIMS ion beam, which typically has a width of 10–30 microns but much finer depth resolution (12), with the sequential measurement of Pb isotopes varying over time as the zircon surface is sputtered at a typical rate of ca. 100 nm per magnet cycle, leading to significant deviations in the estimation of both U–Pb and Pb–Pb ages.

Uranium–Pb zircon ages obtained from SIMS analyses are calculated by calibration against a matrix-matched standard reference zircon. This assumes a similar ablation behavior between the standard and the analyzed material. However, the separation of Pb in zircon into a metallic phase may produce changes in ablation and ionization behavior, especially considering the weakly bonded nature of native lead. Whereas Pb heterogeneity on a submicron scale may only result in increased imprecision in U–Pb and Pb–Pb age estimates, sputtering behavior may induce systematic discordance. Systematic discordance may also be induced by micrometer-scale redistribution of Pb inclusions, as crystallization fronts sweep Pb out of recovered domains and concentrate them in more amorphous domains, as indicated in Figs. 3 and 4. Furthermore, as noted in previous studies (2, 3, 12), if the redistribution of Pb occurred in geologically ancient times, it would have a higher ^{207}Pb/^{206}Pb ratio than any radiogenic lead that accumulated from the time of annealing to the present day. This would inevitably produce reverse discordance of U–Pb and Pb–Pb ages, with spuriously old ^{207}Pb/^{206}Pb age estimates obtained from domains where mobilized radiogenic lead was preferentially concentrated.

The occurrence of metallic Pb nanospheres in zircon affected by UHT metamorphism can explain the unusual U–Pb behavior of such grains during SIMS U–Pb analysis (2, 3, 12). Their formation is related to an annealing process under high-grade conditions, and once formed, the transformation of the enclosing metamict domains into newly crystallized zircon effectively arrests Pb loss, explaining why zircon that has experienced such extreme conditions is not completely reset to its metamorphic age. However, inhomogeneity in the distribution of radiogenic lead, and possible matrix effects, may result in inaccurate age estimates of such zircon when analyzed by microbeam techniques. In samples that contain zircon grains with a uniform age, such inaccuracies can be monitored; however, removed from the

context of their host rock, for example in a detrital population, there is great potential for erroneous age interpretation.

Methods Summary

Six foils of zircon were prepared for TEM study applying the site-specific FIB technique, which allows cutting an electron-transparent foil from preselected areas of interest (31–34). The TEM foils are 15–20-μm wide, 10–15-μm deep, and 100-nm thick. A glass fiber attached to a micromanipulator was used to lift out foils from the excavation sites. Details of the technique are given in ref. 35.

Analytical and energy-filtered high-resolution TEM (HRTEM) using a FEI Tecnai G2 F20 X-Twin at GFZ Potsdam operated at 200 kV with a field emission gun electron source was used for the present study. The TEM is equipped with a postcolumn Gatan imaging filter (GIF Tridiem). The HRTEM images presented were energy-filtered using a 10 eV window on the zero loss peak. Analytical TEM was performed with an EDAX X-ray analyzer equipped with an ultra-thin window. The X-ray intensities were measured in scanning transmission mode, where the electron beam is serially scanned over a preselected area, minimizing mass loss during data acquisition.

ACKNOWLEDGMENTS. We thank Charles Magee, Ian Williams, and Michał Żelechower for discussion and two anonymous reviewers for constructive comments. Samples for this study were provided by Chris Carson from Geoscience Australia and Chris Clark from Curtin University. M.A.K. acknowledges funding support from the European Commission Seventh Framework Programme under the People (Marie Curie Fellowship, PIOF-GA-2010-273412) and RegPot (Research Potential, ATLAB 285989) programs. K.M. acknowledges financial support from the DFG (Deutsche Forschungsgemeinschaft, HE2015/11-1) and the Helmholtz foundation.

1. Bose PP, Mittal R, Chaplot SL (2009) Lattice dynamics and high pressure phase stability of zircon structured natural silicates. *Phys Rev B* 79(17):174301.
2. Kusiak MA, Whitehouse MJ, Wilde SA, Nemchin AA, Clark C (2013) Mobilization of radiogenic Pb in zircon revealed by ion imaging: Implications for early Earth geochronology. *Geology* 41(3):291–294.
3. Kusiak MA, et al. (2013) Changes in zircon chemistry during Archean UHT metamorphism in the Napier Complex, Antarctica. *Am J Sci* 313(9):933–967.
4. Holland HD, Gottfried D (1955) The effect of nuclear radiation on the structure of zircon. *Acta Crystallogr* 8(6):291–300.
5. Nasdala L, et al. (2001) Metamictisation of natural zircon: Accumulation versus thermal annealing of radioactivity-induced damage. *Contrib Mineral Petrol* 141(2):125–144.
6. Murakami T, Chakaumakos BC, Ewing RC, Lumpkin GR, Weber WJ (1991) Alpha-decay event damage in zircon. *Am Mineral* 76(8):1510–1532.
7. Nasdala L, et al. (2002) Annealing radiation damage and the recovery of cathodoluminescence. *Chem Geol* 191(1-3):121–140.
8. Pidgeon R (2014) Zircon radiation damage ages. *Chem Geol* 367:13–22.
9. Cherniak DJ, Watson EB (2003) Diffusion in zircon. *Rev Mineral Geochem* 53:113–143.
10. Meldrum A, Boatner LA, Weber WJ, Ewing RC (1998) Radiation damage in zircon and monazite. *Geochim Cosmochim Acta* 62(14):2509–2520.
11. Utsunomiya S, et al. (2004) Nanoscale occurrence of Pb in an Archean zircon. *Geochim Cosmochim Acta* 68(22):4679–4686.
12. Whitehouse MJ, Kumar GRR, Rimša A (2014) Behaviour of radiogenic Pb in zircon during ultrahigh-temperature metamorphism: An ion imaging and ion tomography case study from the Kerala Khondalite Belt, southern India. *Contrib Mineral Petrol* 168(2):1–18.
13. Valley JW, et al. (2014) Hadean age for a post-magma-ocean zircon confirmed by atom-probe tomography. *Nat Geosci* 7(3):219–223.
14. Black LP, Sheraton JW, James PR (1986) Late Archean granites of the Napier Complex, Enderby Land, Antarctica—A comparison of Rb-Sr, Sm-Nd and U-Pb isotopic systematics in a complex terrain. *Precambrian Res* 32(4):343–368.
15. Harley SL, Black LP (1997) A revised Archaean chronology for the Napier Complex, Enderby Land, from SHRIMP ion-microprobe studies. *Antarct Sci* 9(1):74–91.
16. Kelly NM, Harley SL (2005) An integrated microtextural and chemical approach to zircon geochronology: Refining the Archaean history of the Napier Complex, east Antarctica. *Contrib Mineral Petrol* 149(1):57–84.
17. Harley SL, Motoyoshi Y (2000) Al zoning in orthopyroxene in a sapphirine quartzite: Evidence for >1120°C UHT metamorphism in the Napier Complex, Antarctica, and implications for the entropy of sapphirine. *Contrib Mineral Petrol* 138(4):293–307.
18. Williams IS, Compston W, Black LP, Ireland TR, Foster JJ (1984) Unsupported radiogenic Pb in zircon—A cause of anomalously high Pb-Pb, U-Pb and Th-Pb ages. *Contrib Mineral Petrol* 88(4):322–327.
19. Black LP, Williams IS, Compston W (1986) 4 zircon ages from one rock—The history of a 3930 ma-old granulite from Mount Sones, Enderby Land, Antarctica. *Contrib Mineral Petrol* 94(4):427–437.
20. Lide DR (1983–1984) *Handbook of Chemistry and Physics* (CRC Press, Boca Raton, FL).
21. Garnier P, Moreau J, Gavarri JR (1990) Analyse de rietveld de la structure de Pb1-xTixO1+x par diffraction des neutrons. *Mater Res Bull* 25(8):979–986.
22. Filatov S, et al. (2005) High-pressure synthesis of α-PbO2 and its crystal structure at 293, 203 and 113 K from single crystal diffraction data. *Solid State Sci* 7(11): 1363–1368.
23. Gavarri JR, Weigel D (1975) Oxydes de plomb. I. Structure cristalline du minimum Pb3O4, a temperature ambiante (293K). *J Solid State Chem* 11(4):344–345.
24. Sidra OI, Zenko DS, Krivovichev SV (2014) Structural complexity of lead silicates: Crystal structure of Pb21[Si7O22]2[Si4O13] and its comparison to hyttsjöite. *Am Mineral* 99(3):817–823.
25. Petter W, Harnik AB, Keppler U (1971) Die kristallstruktur von blei-barysilit, Pb3Si2O7. *Zeitschrift fuer Kristallographie* 133(1):445–458.
26. Kogawa M, Watson EB, Ewing RC, Utsunomiya S (2012) Lead in zircon at the atomic scale. *Am Mineral* 97(7):1094–1102.
27. Watson EB, Cherniak DJ, Hanchar JM, Harrison TM, Wark DA (1997) The incorporation of Pb into zircon. *Chem Geol* 141(1-2):19–31.
28. Trachenko K, et al. (2004) Radiation-induced structural changes, percolation effects and resistance to amorphization by radiation damage. *Mater Res Soc Symp P* 792(1): 509–524.
29. Anderson AJ, Wirth R, Thomas R (2008) The alteration of metamict zircon and its role in the remobilization of high-field-strength elements in the Georgeville granite, Nova Scotia. *Can Mineral* 46(1):1–18.
30. Thomas JB, Bodnar RJ, Shimizu N, Chesner CA (2003) Melt inclusions in zircon. *Rev Mineral Geochem* 53:63–87.
31. Lee MR (2010) Transmission electron microscopy (TEM) of Earth and planetary materials: A review. *Mineral Mag* 71(1):1–27.
32. Lee MR, Bland PA, Graham G (2003) Preparation of TEM samples by focused ion beam (FIB) techniques: Applications to the study of clays and phyllosilicates in meteorites. *Mineral Mag* 67(3):581–592.
33. Phaneuf MW (1999) Application of focused ion beam microscopy to materials science specimens. *Micron* 30(3):277–288.
34. Wirth R (2009) Focused Ion Beam (FIB) combined with SEM and TEM: Advanced analytical tools for studies of chemical composition, microstructure and crystal structure in geomaterials on a nanometre scale. *Chem Geol* 261(3-4):217–229.
35. Wirth R (2004) Focused Ion Beam (FIB): A novel technology for advanced application of micro- and nanoanalysis in geosciences and applied mineralogy. *Eur J Mineral* 16(6):863–876.